HARKE: Human Activity Recognition from Kinetic Energy Harvesting Data in Wearable Devices

Sara Khalifa, *Member, IEEE*, Guohao Lan, *Student Member, IEEE*,
Mahbub Hassan, *Senior Member, IEEE*, Aruna Seneviratne, *Senior Member, IEEE*,
and Sajal K. Das, *Fellow, IEEE*

Abstract—Kinetic energy harvesting (KEH) may help combat battery issues in wearable devices. While the primary objective of KEH is to generate energy from human activities, the harvested energy itself contains information about human activities that most wearable devices try to detect using motion sensors. In principle, it is therefore possible to use KEH both as a power generator and a sensor for human activity recognition (HAR), saving sensor-related power consumption. Our aim is to quantify the potential of human activity recognition from kinetic energy harvesting (HARKE). We evaluate the performance of HARKE using two independent datasets: (i) a public accelerometer dataset converted into KEH data through theoretical modeling; and (ii) a real KEH dataset collected from volunteers performing activities of daily living while wearing a data-logger that we built of a piezoelectric energy harvester. Our results show that HARKE achieves an accuracy of 80 to 95 percent, depending on the dataset and the placement of the device on the human body. We conduct detailed power consumption measurements to understand and quantify the power saving opportunity of HARKE. The results demonstrate that HARKE can save 79 percent of the overall system power consumption of conventional accelerometer-based HAR.

Index Terms—Wearable computing, energy harvesting, human activity recognition, internet of things

---

1 INTRODUCTION

WITH the rapid advancement of electronics, wearable devices such as Fitbit, Apple Watch, and Nike Fuel-Band, are rapidly becoming an integral part of our daily lives. A key service provided by these devices is to continuously track the movements and activities of the users with the help of inbuilt precision accelerometers enabling 24x7 activity information at the finger tip of the user. While health and fitness are two major application domains [1], [2], [3], [4], continuous activity monitoring using some form of wearable devices has also potential applications in many other domains, such as sports [5], smart living [6], and indoor positioning [7], [8], [9], [10].

Despite the growing demand for wearable devices, battery recharging is seen as a major roadblock to the ultimate pervasiveness of this technology. Although battery technology has advanced over the years, most wearable devices still require battery recharging every other day or at least once a week. To reduce dependance on batteries, a current trend in the literature [11], [12], [13], [14] is to develop kinetic energy harvesting (KEH) solutions to convert kinetic energy released from human motion and activities into usable electrical energy to power wearable devices. Some wearable

KEH products are already appearing in the market, such as AMPY[1] and EnSole,[2] that enable the wearers to capture and convert kinetic energy as they walk, run, and jog into battery power that can be used by their smartphones and wearables. These recent developments paint a promising picture for the inclusion of KEH in many future wearable products.

While the mainstream energy-harvesting research focuses on increasing the power throughput of the energy-harvesting hardware, in this paper, we investigate a different approach to exploiting KEH for human activity recognition (HAR). In particular, we propose to *mine the energy harvesting patterns to detect human activities*. The feasibility of such mining relies on the fact that human motion is the source of any power generated by the wearable KEH hardware and that human motion has distinctive patterns for different human activities. Indeed, state-of-the-art wearable-based HAR technology [15], [16], [17], [18], [19], [20], [21] relies on these distinctive motion patterns that are accurately captured by three-axial accelerometers.

However, accelerometers require constant power supply for sampling acceleration data from human motion, which could be avoided if activity was recognised directly from the output pattern of the KEH device. Therefore, KEH could potentially serve the dual purpose of generating power as well as saving sensor-related power consumption by acting as a proxy for the accelerometer. The concept of human activity recognition from kinetic energy is referred to as HARKE in this paper, while the state-of-the-art HAR methods that classify activities using accelerometer data are referred to as HARAC. Although HARAC is a matured technology, there

- S. Khalifa, G. Lan, M. Hassan, and A. Seneviratne are with the University of New South Wales, and Data61—CSIRO, Sydney, NSW 2052, Australia. E-mail: {s.khalifa, g.lan, mahbub.hassan, a.seneviratne}@unsw.edu.au and {sara.khalifa, guohao.lan, mahbub.hassan, aruna.seneviratne}@data61.csiro.au.
- S. K. Das is with the Department of Computer Science, Missouri University of Science and Technology, Rolla, MO 65409. Email: sdas@mst.edu.

1. AMPY: http://www.getampy.com (accessed on July 28th 2016).
2. EnSole: http://www.solepowertech.com (accessed on July 28th 2016).

is little known about the potential of HARKE. In our recent study [22], we applied theoretical modelling to estimate KEH patterns from accelerometer patterns of common human activities using mass-spring damping system. We used the estimated KEH data to prove the concept of using KEH signal as a source of sensing human activities.

In this paper, we carry out more comprehensive study to assess the potential of KEH as a sensor for realising human activities. First, we use a publicly available dataset [23] that contains 3-axis acceleration data collected from eight subjects mounting the sensing units on three different body positions (arm, leg, and torso) and performing nine daily and sport activities, such as rowing, cycling, running, walking, jumping , standing, sitting, ascending, and descending stairs. The KEH data for all of these activities and body placements were approximated by applying a standard mass-spring damping system to the available acceleration data.

Then, we build a wearable KEH datalogger capable of logging both accelerometer as well as voltage output of a piezo-electric KEH device that harvests electrical energy from the vibrations of the piezoelectric element. We collect both accelerometer and piezoelectric voltage data from ten subjects performing five daily activities, such as walking, running, standing, ascending and descending stairs, by wearing the datalogger at two different body placements, hand and waist. Our analysis shows that HARKE is sensitive to both body placements and classifiers used with significant accuracy differences. We identify a vibration-specific feature set which noticeably improves HARKE performance.

Moreover, we compare the performance of HARKE with the conventional state-of-the-art HARAC. We observe that HARKE is as accurate as HARAC so long as the activities are not too similar, but the performance of HARKE would start to deteriorate as soon as very similar activities are added to the target set. This leads to approximately 15 percent performance gap with HARAC when the device is attached to the hand or arm. However, the gap is significantly reduced to only 4.17 percent when the device is placed closer to the central part of the body which helps sensing and identifying similar activities more accurately.

The contributions of this paper can be summarised as follows:

- We present a novel human activity recognition method (called HARKE) which uses KEH patterns as the source for activity classifications.
- We provide a proof of concept of HARKE by implementing the idea with off-the-shelf energy harvesting hardware and experimenting it with real subjects. We show that HARKE can detect some basic activities of daily living with 80 to 95 percent accuracy depending on the placement of the device on the human body.
- We conduct a detailed power measurement study to understand and quantify the power saving opportunity of HARKE. We demonstrate that HARKE can save 79 percent of the overall system power consumption compared to the conventional accelerometer-based HAR.

The rest of the paper is organised as follows. Related work is reviewed in Section 2 followed by the preliminaries on the accelerometers and KEH principles in Section 3. The motivation of HARKE and the proposed architecture is presented in Section 4. Next, Section 5 presents the evaluation of HARKE using a publicly available accelerometer dataset which is converted into KEH data using a standard mass-spring damping system. Section 6 presents HARKE experiments with wearable KEH hardware. Finally, the power consumption measurements are explained in Section 7, while conclusions and future research directions are offered in Section 8.

2 RELATED WORK

Existing human activity recognition (HAR) systems can be broadly categorized into three different approaches [24], vision-based, environmental-based and wearable-based. Vision-based HAR, which is achieved by instrumenting the environment with cameras, has been a research focus for a long period of time due to its important role in various domains such as surveillance, security, and robot learning [25], [26]. However, the deployment and maintenance of cameras (as recording devices) are costly in addition to the privacy and ethical issues [24].

Similarly, environmental-based HAR uses physical sensors (e.g., pressure, proximity, RFID, etc.) attached on objects to infer human activities from interaction with objects or change of environmental variables [27]. It enables many useful applications in smart environments domain including people/object tracking [28] and detection of human-object interaction [29]. In particular, RFID-based HAR [30], [31] which relies on body attenuation and/or channel fading of wireless radio, has many power advantages with RF energy harvesting [32], [33]. However, the recorded RFID data is highly subject to noise and interference caused by moving people and other objects which in turn impacts the performance of HAR using this approach [34]. Moreover, it only recognizes those activities that involve interaction between human and objects [34].

On the other hand, wearables can continuously monitor user activities at all times and locations. By placing various wearables on the human body, accurate and pervasive HAR can be achieved without deploying significant infrastructure and at the same time preserving the privacy of users [35]. Several previous studies relied on attaching various specialised wearable sensors to different places on the human body to achieve HAR [15], [16], [17], [18]. However, the recent popularity of smart wearables, such as smart-phones, smart-glasses, and smart-watches, has shifted the research attention to use such wearables for HAR [19], [20], [21]. The major challenge of wearable devices is the battery life, especially with increasing user demand for more power and functionality. It is not convenient for many users to frequently recharge their wearable devices, especially if they need to plug these devices into a power source. Although, there exists extensive work on improving battery technology to meet the users' expectations, batteries are still one of the biggest limitations in advancing the wearable technology [36].

Accordingly, minimising the power consumption of wearables has become an essential requirement. Three main components are highly contributing to the power consumption of the wearables: sensing, computation, and communication. Reducing the power consumption of these components can make the wearable more energy efficient. Typically, wearable-based HAR relies on inertial sensors (e.g., accelerometers) to measure the acceleration while performing different activities. Informative features are then extracted from the accelerometer data and used to train a classifier, which is used later to detect activities

from a given sample of acceleration values. Although inertial sensors can be considered low-power electronics, the continuous sampling of different inertial sensors in the wearable can be power consuming. Therefore, in this paper we focus on reviewing some of the ideas from the literature that aim to reduce the sensors-related power consumption in wearable devices.

Sensor reduction. It has been found that reducing the number of sensors for activity recognition can help improve the energy efficiency of the device, but it can trade off the detection accuracies. A dynamic sensor selection mechanism is therefore preferred to provide energy efficiency while achieving the desired performance of the detection algorithms. For example, Zappi et al. [37] exploited sensor redundancy for dynamically selecting sensors according to their contribution to the classification accuracy as assessed during system training. By reducing the average number of sensors used, their method was able to significantly extend the battery life while maintaining high accuracy for HAR. Wang et al., [38] selectively turned on the minimum set of sensors to monitor user state and triggered a new set of sensors only if necessary to achieve state transition detection. Gordon et al., [39] leveraged the predictability of human behavior to turn off sensors which are needed to recognise only the unlikely activities.

Adaptive sampling. Because the system power consumption increases with the increase in sampling rate, reducing the sampling rate of sensors has become a popular method to reduce power consumption of HAR. However, any reduction in sampling rate must be achieved without sacrificing the precision of the recognition system. Krause et al., [40] studied the trade-off between sampling rate (power consumption) and human activity classification accuracy for the eWatch wearable device. The authors have demonstrated that the battery life of the device can be extended significantly by selecting the optimal sampling rate without sacrificing accuracy. This study indicates the existence of a sampling threshold, below which the accuracy falls dramatically. Consequently, the use of a sampling rate equal to the sampling threshold is proposed in order to save energy. In [41], Yan et al., pointed out that the trade-off is activity-specific, and proposed that the sampling frequency and classification features should be adapted in real time, based on the activity type. Moreover, in [42], Qi et al., proposed AdaSense algorithm which uses a lower power single activity event detection most of the time and only resorts to higher power multi-activity classification when the activity changes. AdaSense uses Genetic Programming to find the optimal feature set that effectively reduces the sampling rate and computational complexity.

KEH Wearables. Although sensor reduction and adaptive sampling mechanisms can reduce the sensor-related power consumption and extend the wearable lifetime, battery-powered wearables cannot provide sustained operation without the need for battery recharge and eventually replacement. Recently, Kinetic Energy Harvesting has emerged as a viable option to power the wearables by converting the kinetic energy from human motion into electrical energy [43]. Some wearable KEH products are already appearing in the market, such as AMPY and EnSole, that enable the wearers to capture and convert kinetic energy as they walk, run, and jog into battery power to be used by their smartphones and wearables. However, the amount of power that can be harvested from daily human activities with current energy harvesting hardware is still too small to

enable wearables or smartphones to fully rely on KEH to power them. Many KEH models have been recently developed [11], [12], [13], [14]. The main focus of these models is to optimise the parameters of the harvester so as to maximise the output harvested power. However, there is still a gap between what energy can be generated and what energy is required to power the wearables. This is particularly true with the function rich wearables consisting of various embedded sensors.

In our recent study [22], we showed that the power requirement for sampling an accelerometer to detect common human activities with high accuracy ranges between 0.35 to 5 times the harvested kinetic power from human motion. Although reducing the sampling rate of accelerometer can save some power, accelerometers still require power supply during sampling. To address this challenge, we proposed the prospect of using KEH signal as a source of sensing human activities, which leads to further opportunity of power saving. We estimate KEH patterns from accelerometer patterns for common human activities using theoretical modeling. In [44], a discussion about KEH wearables for activity-aware services is provided with a preliminary proof of concept experimental study. In this paper, we carry out more extensive experiments to assess the potential of KEH as a sensor for realising HAR using a range of common daily activities and different placements of the KEH device on the human body. We also conduct measurements to quantify the power saving opportunity of our method as compared to the existing accelerometer-based method.

3 ACCELEROMETER AND KEH PRELIMINARIES

Both accelerometers and KEH transducers rely on the same basic principle of mass-spring damping system, however, they serve different purposes. Accelerometers are used to sense vibration, but KEH is used to generate electrical energy from the wasted vibration energy. Generally speaking, accelerometers require some means for inferring acceleration from sensed vibration. In this section, we present some preliminaries on accelerometers and KEH.

3.1 Accelerometers

Accelerometers are electromechanical devices that are used to sense static acceleration forces such as gravity and/or dynamic acceleration forces such as vibrations and movement. They can sense acceleration in one, two, or three axes. Different kinds of accelerometers are available, however, capacitive accelerometers are mostly used in wearable and mobile devices. This is because they have low power consumption, large output level, low noise level, and fast response to motions [45]. In a capacitive accelerometer, a capacitor is formed by a *stationary plate* (the housing which moves with the base acceleration) and a *moving plate* attached to the seismic mass. The distance between these two plates determines the capacitance, which can be monitored to infer acceleration (change in capacitance is related to acceleration). Capacitive accelerometers are capable of measuring constant acceleration, such as gravity as well as slow transient and periodic acceleration. Accelerometers are generally considered low-power devices which require a power supply voltage of 5V or less. Their required current can vary depending on the settings of power saving mode or standard operating mode and typically ranges between micro and milli ampere [46].
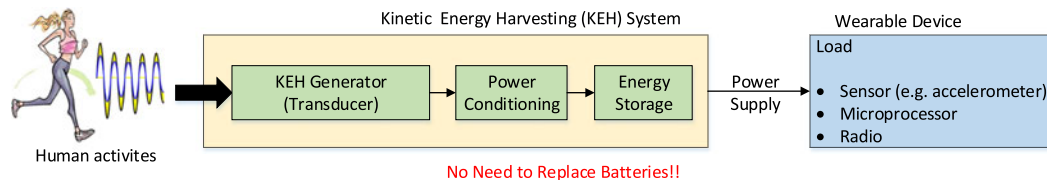
Fig. 1. A generic architecture of a KEH-powered wearable device.

3.2 Kinetic Energy Harvesting

Kinetic energy harvesting is a process of converting the environmental kinetic or vibration energy into electrical energy which can be stored to power small and low energy electronics. KEH can ease the dependence on batteries and significantly enhance the versatility of consumer electronics. Kinetic and vibration energy harvesting are synonyms; the environment around us is full of sources of kinetic or vibration energy such as natural seismic vibration (e.g., earthquakes), wind movement, sea waves, vehicular traffic, machinery vibration and human motion. Among these environmental vibration options, human motion is the most relevant for wearables because it can power the wearable directly from human movements. Fig. 1 shows a generic architecture for a KEH-powered wearable device. The KEH system typically contains a generator (transducer) to convert human motion into electrical power, a power conditioning circuit to provide power rectification and regulation, and a storage element (e.g., a capacitor or a rechargeable battery) to store the harvested energy. The harvested energy is used to extend the life time of batteries, thus enabling self-powered wearables.

There are three main transduction mechanisms for converting kinetic energy to electric power [47]: piezoelectric, electromagnetic (capacitive), and electrostatic (inductive). Piezoelectric is the most favourable transduction mechanism due to its simplicity and compatibility with MEMS or micro electrical mechanical system [48]. The piezoelectric effect was discovered in natural quartz crystals, but today's piezoelectric transducers are typically made from patented proprietary ceramics. Fig. 2 shows a typical usage configuration of a piezoelectric cantilevered beam. One end of the beam is fixed to the device, while the other is set free to oscillate (vibrate). When the piezoelectric material is subjected to a mechanical stress due to any source of environmental vibration, it expands on one side and contracts on the other. Positive charges accumulate on the expanded side and negative charges on the contracted side, generating an alternating current (AC) voltage as the beam oscillates around the neutral position. The amount of voltage is proportional to the applied stress, which means that different vibration patterns generate different AC voltage patterns.
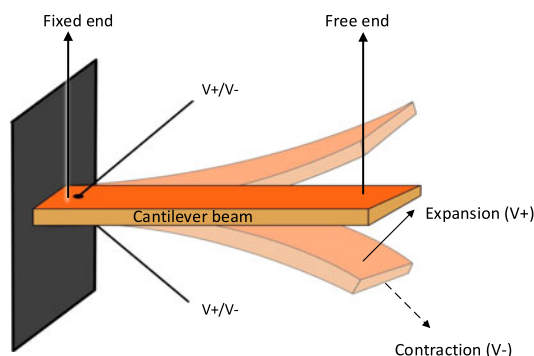

Fig. 2. The piezoelectric cantilevered beam.

The AC voltage is usually converted into regulated direct current (DC) which is suitable to power sensor nodes, microcontrollers, and peripherals.

4 PROPOSED HARKE ARCHITECTURE

Fitness trackers and wearable health monitoring systems are expected to have long operation time, as it is definitely not convenient for elders and patients to charge their health monitoring device frequently. In the near future, kinetic energy harvesters can be integrated to these devices to extend the battery lifetime and achieve long-term activity monitoring. In light of this, we envision and propose HARKE which eliminates the need for powering an accelerometer to sense human activity. Instead, it employs kinetic energy harvesting and infers human activity directly from the KEH patterns without using any accelerometer.

Fig. 3 shows the general architecture of HARKE, in which the wearable health monitoring system is mainly used to continuously collect the KEH data generated from human motion, and periodically transmit them to the data center (e.g., a data server of a healthcare company) for further analysis and activity classification. In the server, the KEH data are processed and analyzed to extract informative features. Then, the extracted features are used to train and validate a classifier model which will be used to recognize human activities from KEH patterns. The proposed use of KEH patterns for classifying human activities is based on the observation that different activities produce kinetic energy in a different way leaving their signatures in the harvested power signal.

The fundamental advantage of HARKE is the energy saving due to elimination of the need for powering an accelerometer to sense human activity. HARKE samples only a transducer that remains active all the time without requiring any power supply and generates a single-axial data trace to be transmitted. On the other hand, HARAC requires powering up an accelerometer for each sensor sampling which generates three times of data samples (3-axial accelerometer) to be transmitted. This indicates that HARKE can significantly reduce the power consumption of both data sampling and wireless transmission, thereby extending the life time of resource-constrained wearable health monitoring devices. In the next two sections, we evaluate the performance of HARKE using two independent datasets. Then, in Section 7 we quantify the energy saving opportunity of HARKE as compared to HARAC.

5 EVALUATING HARKE WITH PUBLIC DATASET

In this section, we make use of a public activity dataset [23] to evaluate the proposed HARKE architecture. We use a
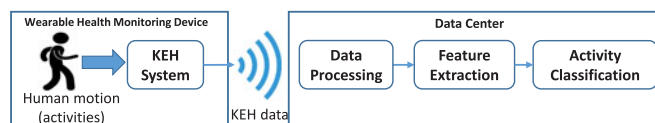

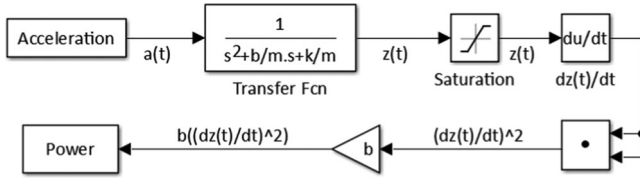
Fig. 3. Proposed HARKE architecture.

Fig. 4. Simulink blocks to estimate KEH power from accelerometer data.

mathematical model that relies on the most basic principle of a kinetic energy harvester [14], namely a standard mass-spring damping system, to estimate the kinetic power signal that could be harvested by a kinetic energy harvester.

5.1 Motion Dataset

This dataset contains 3-axial acceleration measurements collected from eight subjects (four females and four males, ages from 20 to 30) performing a variety of daily and sports activities [23]. We study nine activities including rowing (ROW), cycling on an exercise bike (CYC), running on a treadmill with a speed of 8 km/h (RUN), walking on treadmill with a speed of 4 km/h (WALK), jumping (JUMP), standing (STAND), sitting (SIT), ascending stairs (SU), and descending stairs (SD). The sensing units were mounted on three different body placements (Arm, Leg, and Torso), with a 25 Hz sampling frequency.

5.2 Derivation of KEH Data

We apply the mathematical model developed in [12], [14] to estimate the KEH power from the acceleration traces in the dataset. Typically, a resonant kinetic energy harvester is represented by a mass-spring damper equivalent model whereby the linear damper represents the combined damping offered by electrical and mechanical domains. The mass-spring damper system is a second order system, which is commonly encountered in system dynamics and can be modeled using two methods: a second order ordinary differential equation, and a conventional transfer function. The second order differential equation governing the system is given by

$$m\ddot{z}(t) = a(t) - b\dot{z}(t) - kz(t),\qquad(5)$$

where m is the *proof* mass, k is the spring constant, b is the damping factor, $a(t)$ is the external input (control force), $\dot{z}$ and $\ddot{z}$ are the first and second derivatives of the output variable $z(t)$.

Equation (5) can also be represented as a transfer function (in the Laplace domain) as follows:

$$z(t) = \mathcal{L}^{-1} Z(s) = \mathcal{L}^{-1}\left(\frac{A(s)}{s^2 + \frac{b}{m}s + \frac{k}{m}}\right),\qquad(6)$$

where $A(s)$ and $Z(s)$ denote, respectively, the Laplace transforms of $a(t) = \sqrt{a_x(t)^2 + a_y(t)^2 + a_z(t)^2}$, the overall magnitude of the acceleration, and the proof mass displacement $z(t)$. Maximum power is achieved when the excitation (input) frequency is equal to the natural frequency of the system. All practical systems dissipate energy when they vibrate. To account for this, damping must be considered. Therefore, the transfer function in Equation (6) can be represented in terms of the natural frequency $\omega = \sqrt{\frac{k}{m}}$ and the damping coefficient $\zeta = b/(2\sqrt{k*m})$, as follows:

$$\frac{Z(s)}{A(s)} = \frac{1}{s^2 + 2\zeta\omega s + \omega^2}.\qquad(7)$$

Once the gravity is filtered out from the motion data, the filtered motion data is converted to *proof mass displacement* using the Laplace domain transfer function of Equation (6). Next, the resulting proof mass displacement, $z(t)$, is bounded by the limit of the proof mass displacement, Z_L. Finally, the generated harvested power is determined by

$$p(t) = b\dot{z}^2(t).\qquad(8)$$

We used the following configuration values: $m = 10^{-3}kg$, $Z_L = 10mm$, $k = 0.17$, and $b = 0.0005$, optimised in [14] for typical human activities. The entire procedure was implemented using MATLAB and SIMULINK [49]. The simulink blocks of this model are shown in Fig. 4. Fig. 5 shows the accelerometer patterns and the corresponding power traces for nine activities and three placements of the device on the human body: arm, leg, and torso. As shown, like accelerometer, the KEH power samples exhibit different patterns for different activities. These patterns will be used in the performance evaluation presented in Section 5.4.

5.3 Feature Extraction and Classification

Feature extraction is a critical initial step in any classification process. This step is responsible for extracting the hidden information from the input raw data in order to perform the desired task.

The input raw data is usually subject to noise due to random and short-term movements derived from hand shaking and user interactions. To eliminate the interference of such noise, we first smooth the data using a moving average filter which is simple but effective for removing random noise from time series. It smooths the data traces by replacing each data point with the average of the neighboring data points defined within the span (we use a span of 3 data points). Next, we consider a technique of *window overlapping* to segment the input data traces into the corresponding activity segments. In this technique, the data traces are subdivided into smaller windows, and then the features are extracted from the consecutive windows. Using overlapping windows is a common practice to reduce the information loss at the edges of the window. In this paper, we used windows of 5 seconds with 50 percent of overlap between consecutive windows.

Table 1 presents the features used in our study. It shows 24 features that are commonly used for HARAC, that is accelerometer-based HAR. As the accelerometer generates three time series along the x-, y-, and z- axes, some features are extracted from each axis separately (single-axial features) and some are extracted as a combination between the three axes (multi-axial features). Table 1 includes 19 single-axial features and 5 multi-axial features. For accelerometer signal, the single-axial features are extracted from each axis separately, giving a total of 57 features, in addition to the 5 multi-axial features extracted as a combination between the three axes, thus giving a total of 62 features. On the other hand, the KEH signal has only one axis of AC voltage, resulting in a total of 19 single-axial features. Overall, we extracted a total of 62 features from the acceleration signal and 19 features from the KEH signal. We call this as the Original Feature Set (OFS).

Based on the success of other researchers in classifying a range of human activities using accelerometer data, we chose four common classifiers to evaluate the recognition
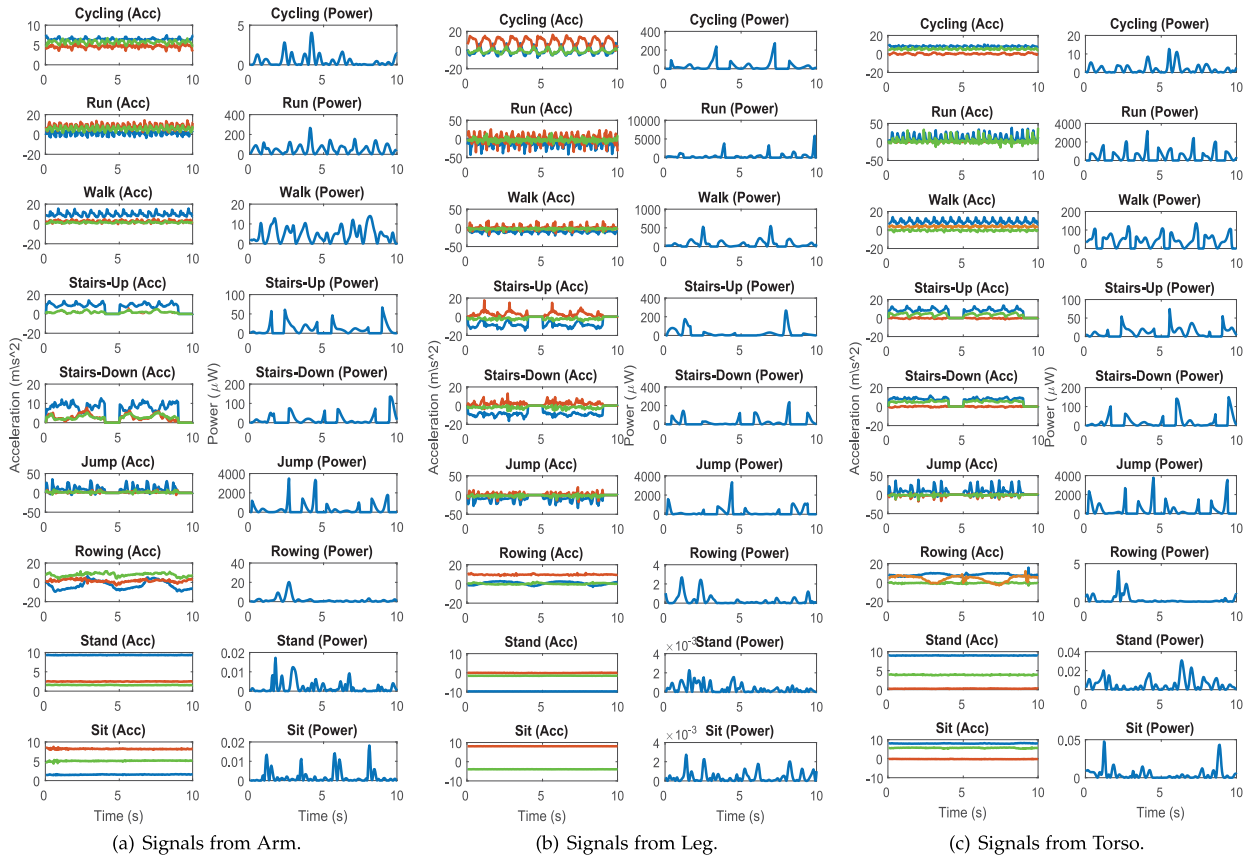
Fig. 5. Acceleration and the corresponding estimated power signals for different activities ("Acc" means Acceleration).

accuracy of HARKE: (1) C4.5 Decision Tree (DT) [50]; (2) IBk Nearest Neighbour (NN) [51]; (3) Naive Bayes classifier with kernel estimation; and (4) Support Vector Machine (SVM) [52]. We utilize the widely used and publicly available machine learning platform called Waikato Environment for Knowledge Analysis (WEKA) [53] to assess the performance of HARKE and compare it to HARAC.

5.4 Performance Results

Table 2 presents the achieved recognition accuracies of both HARKE and HARAC at three body placements–Arm, Leg and Torso. We observe that HARAC, which exploits acceleration information from three different axes, achieves high recognition accuracies (above 93 percent) irrespective of the classifier selection and body placement. Torso placement achieves the best accuracy ($\approx 99\%$) with no significant differences between the four considered classifiers. In contrast, HARKE performance is sensitive to both body placements and classifiers used to detect activities with significant accuracy differences. For HARKE, the Decision Tree (DT) classifier appears to outperform all other classifiers with recognition accuracies of 80.96, 82.72, and 95.37 percent for Arm, Leg, and Torso positions, respectively.

To gain more understanding of the performance of both HARAC and HARKE, we show the True Positive (TP) rate for each recognized activity when the DT classifier is used in Fig. 6. The results are shown for both HARAC and HARKE for the three body placements: Arm, Leg, and Torso. We can see that HARAC achieves more than 0.9 TP rate for all activities and body placements. On the other hand, with HARKE, some activities cannot be detected with high TP rate such as SU and SD in case of Arm position (when it achieves less

than 0.7 TP rate), and STAND and SIT for Leg position (when it achieves less than or equal to 0.7 TP rate). This means that the energy harvesting signal, which is derived from the 3-axial accelerometer signal, does not contain all the information available in the 3-axial accelerometer signal.

This leads to the better performance of HARAC over HARKE. To get a sense of the overall performance difference between HARAC and HARKE, we use the term *accuracy gap* which is defined as the difference (absolute value) between the overall recognition accuracies of both HARKE and HARAC. By calculating the difference between the accuracies of HARKE and HARAC shown in Table 2 for the best classifier (Decision Tree), we find an accuracy gap of 15.23 percent for Arm position and 14.96 percent for Leg position. When Torso position is considered, this problem is resolved and the accuracy gap is reduced to only 4.17 percent. Fig. 6 confirms this outcome by showing TP rate above 0.9 for all activities when the Torso position is considered with HARKE. This means that Torso is the position where the least amount of information is lost and hence HARKE could achieve comparable performance to HARAC.

So far, we have analysed the performance of HARKE using a transformation signal derived from the acceleration data. To assess the validity of these observations, we carry out experiments with a real energy harvesting device as discussed in the next section.

6 EXPERIMENTATION WITH KEH HARDWARE

We further evaluate the proposed HARKE architecture using practical KEH data. The details of the hardware setup, data collection campaign, and evaluation results are presented in this section.

TABLE 1
The Original Feature Set (OFS)

		Feature	Abbreviation	Description
Single-axial features	Time-domain features	mean	mean	The central value of a window of samples.
		variance	var	Measures the amount of variation or dispersion from the mean.
		standard deviation	std	The square root of the variance.
		minimum	min	The minimum value in a window of samples
		maximum	max	The maximum value in a window of samples
		range	range	The difference between the maximum and the minimum values in a window of samples.
		Absolute Mean	absMean	Average of absolute values.
		Coefficient of Variation	CV	A ratio of standard deviation and mean times 100; measure of signal dispersion.
		Skewness	skew	Measure of asymmetry of the probability distribution of the window of samples.
		Kurtosis	kurt	Measure of peakedness of the probability distribution of the window of samples.
		Quartiles: 1st Quartile	Q1	
		2nd Quartile	Q2	Measures the overall distribution of the signal samples over the window.
		3rd Quartile	Q3	
		Inter Quartile Range	IQR	The difference between the upper (third) quartile and the lower (first) quartile of the window of samples; it also measures the dispersion of the signal samples over the window.
		Mean Crossing Rate	MCR	Measures the number of times the signal crosses the mean value; captures how often the signal varies during the time window.
		Absolute Area	absArea	The area under the absolute values of the signal samples. It is the sum of absolute values of the signal samples over the window.
	Frequency-domain features	Dominant Frequency Ratio	DFreqR	It is calculated as the ratio of highest magnitude FFT coefficient to the sum of magnitudes of all FFT coefficients.
		Energy	FDEnergy	It is a measure of total energy in all frequencies. It is calculated as the sum of the squared discrete FFT component magnitudes.
				$$FDEnergy = \sum_{i=1}^{L/2} F_i^2 \qquad (1)$$ where F_i is the magnitude of FFT coefficients.
		Entropy	FDEntropy	Captures the impurity in the measured data. It is calculated as the information entropy of the normalized values of FFT coefficient magnitude.
				$$FDEntropy = -\sum_{i=1}^{L} Fn_i log_2(Fn_i) \qquad (2)$$ where Fn_i is the normalized value of FFT coefficient magnitude.
Multi-axial features	Time-domain features	Total absolute area	TAA	Sum of the absolute areas of all three axes.
				$$TAA = \sum_{i=1}^{L} |Acc_x| + |Acc_y| + |Acc_z| \qquad (3)$$ where $|Acc_x|$, $|Acc_x|$, and $|Acc_x|$ are the absolute values of the three axes of the accelerometer x, y, and z respectively. L is the length of the window.
		Total magnitude area	TMA	The signal magnitude of all accelerometer signal of three axis averaged over the time window.
				$$TMA = \frac{\sum_{i=1}^{L} \sqrt{Acc_x^2 + Acc_y^2 + Acc_z^2}}{L} \qquad (4)$$
		Correlation: Corr(X,Y)	CorrXY	It measures the dependence relationship between two axes of the accelerometer signal.
		Corr(X,Z)	CorrXZ	
		Corr(Y,Z)	CorrYZ	

6.1 Hardware Setup

Our datalogger hardware includes a product called Volture v25w from MIDÉ,[3] which implements the KEH transducer and provides AC voltage as its output. It employs a cantilever that attaches to a piezoelectric crystal. When vibrations set the cantilever in motion, it generates an AC voltage. Volture v25w is sensitive to the vibration frequency range 40 Hz - 120 Hz and it is able to generate a maximum of 34 mW at 80 Hz. Since human motion frequency is rarely higher than 3 Hz, the output power is expected to be a few magnitudes lower. We used a 7 g mass to make the harvester sensitive to lower frequencies. The mass is placed at the free oscillating tip of the cantilever as shown in Fig. 7c. We also added a tri-axial accelerometer (MMA7361LC) to collect the acceleration signal simultaneously for comparison.

3. http://www.mide.com

TABLE 2
Accuracy (%) of Both HARAC and HARKE at
Three Body Placements When OFS is Used

Classifier	HARAC			HARKE		
	Arm	Leg	Torso	Arm	Leg	Torso
DT	96.19	97.68	99.54	80.96	82.72	95.37
NN	94.67	96.87	99.14	61.27	70.36	92.74
NB	93.22	96.95	99.25	67.14	75.85	85.02
SVM	95.04	97.19	99.09	55.64	63.48	75.62

(a) HARAC

	RUN	JUMP	ROW	CYC	WALK	SU	SD	STAND	SIT
Arm	0.9906	0.9886	0.9928	0.9706	0.9175	0.9401	0.9465	0.9953	0.915
Leg	0.9896	0.9923	0.9931	0.9958	0.9675	0.9815	0.9789	0.9964	0.8966
Torso	0.9948	0.9948	0.9938	0.9953	0.9948	0.9959	0.9964	0.9933	0.9995

Activity
(a) HARAC

(b) HARKE

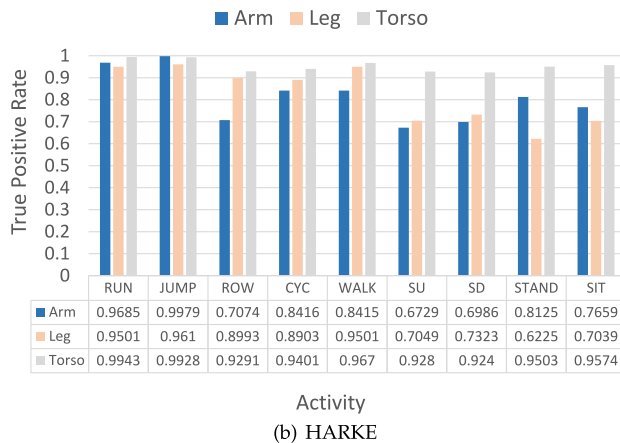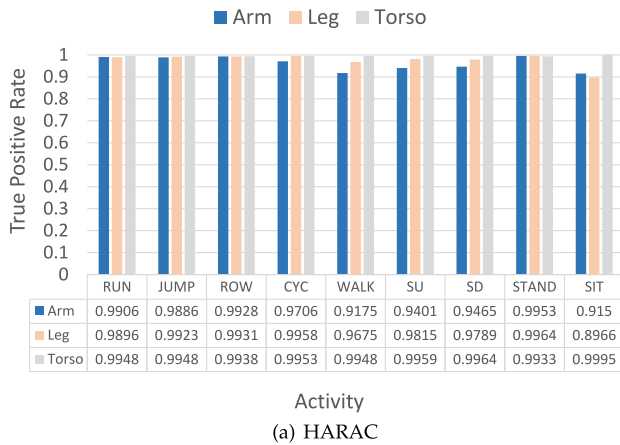|	RUN	JUMP	ROW	CYC	WALK	SU	SD	STAND	SIT
Arm	0.9685	0.9979	0.7074	0.8416	0.8415	0.6729	0.6986	0.8125	0.7659
Leg	0.9501	0.961	0.8993	0.8903	0.9501	0.7049	0.7323	0.6225	0.7039
Torso	0.9943	0.9928	0.9291	0.9401	0.967	0.928	0.924	0.9503	0.9574

Activity
(b) HARKE

Fig. 6. True Positive (TP) rate of each activity when decision tree (DT) classifier is used for: (a) HARAC and (b) HARKE.

The Arduino Uno is used to sample the data from the KEH transducer and accelerometer at 1KHz sampling frequency. The sampled data is saved on an 8 GB microSD card which is connected to the Arduino using microSD shield. A 9V battery is used to power the device. Our hardware also includes two switches–one to switch the device on or off, and the other to control the start and stop of data logging. Figs. 7a, 7b, and Fig. 7c shows the external appearance, the circuit diagram, and the internal appearance of the datalogger, respectively. In the circuit diagram, a 750 KΩ load resistor was soldered at the harvester output to obtain the AC voltage and 2×10 KΩ resistors to make the offset at 2.5 V instead of 0, to access the negative side of the AC voltage. Once the device is assembled, it can be attached to different parts of the subject under test to gather the data.
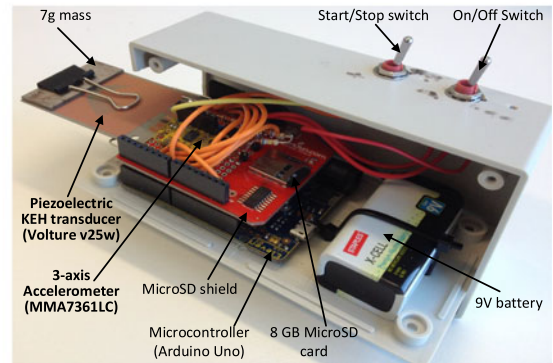
6.2 Output Transformation

The Arduino board has 10 bits of output resolution (i.e., 1024 different values). Therefore, the range of the output
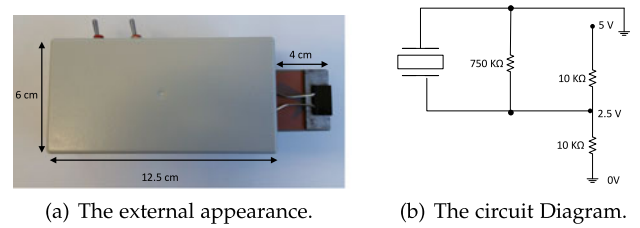
(a) The external appearance.

(b) The circuit Diagram.

(c) The internal appearance.

Fig. 7. The datalogger hardware setup: (a) the external appearance of the data logger, (b) the circuit diagram, and (c) the internal appearance of the data logger.

measurements is from 0 to 1023. We map the range of the measurements to the actual voltage range $(0 - 5V)$ by

$$Voltage = \frac{5 \times m}{1023}, \tag{9}$$

where m is the measurement sampled by the Arduino. For the accelerometer output, we then used the following equation to calculate the corresponding acceleration of the three axes.

$$Acceleration = \frac{Voltage - 1.65}{0.8}, \tag{10}$$

where 1.65 is the 0g acceleration, which is usually defined as half the supply voltage (in this case 3.3V) and 0.8 is the scaling factor between the measured voltage and acceleration in g. Then we divide Equation (10) by 9.81 to get the acceleration in m/s^2. Finally, we subtract 2.5 from the Volture output to compensate changing the Volture offset to $2.5V$ instead of $0V$ in the hardware setup. The Volture's offset has been changed in the design to allow accessing the negative samples of the AC voltage.

6.3 Data Collection

We used the datalogger to collect data from ten different subjects who volunteered to participate in this study. The data includes diversity in gender (4 male and 6 female), age (ranges from 26 to 35), weight (from 58 to 91 Kg), and height (from 154 to 185 cm). We considered five different activities: standing (STAND), walking (WALK), running (RUN), going up stairs (SU), and going down stairs (SD). All subjects performed the activities normally in their own way without any instruction. We considered two different placements to study the impact of device placement on the system performance. The subjects were asked to first hold the datalogger in either their left or right hand, perform the five mentioned activities, and then repeat the same process with the waist placement. Figs. 8 and 9 show the data collection

Fig. 8. Data collection process: (a) Standing (STAND), (b) Walking (WALK), (c) Running (RUN), (d) Going up the stairs (SU), and (e) Going down the stairs (SD).

process of the five activities and the two placements of the device on the subject's body, respectively.

For each subject, we have collected 300 seconds of data for both standing and walking; 240 seconds of data for running; and 200 seconds for both going up and down stairs at each of the two body placements (hand and waist). Figs. 10 and 11 show the accelerometer and KEH patterns, respectively, for the five activities at two body placements.

6.4 Feature Selection

In addition to the OFS (Table 1) used earlier, we now investigate the utility of some additional features presented in Table 3, which are typically used to quantify the severity of vibration [54]. We will call the features in Table 3 the Vibration Feature Set (VFS), which are single-axial features extracted from either the KEH signal or each of the 3-axis acceleration signals. Adding the VFS to the OFS gives a total of 83 features extracted from the accelerometer signal and a

Fig. 9. Device placements on the person's body: (a) hand and (b) waist.

total of 26 features extracted from the KEH signal. We divide the data traces into 5 seconds windows with 50 percent of overlap between consecutive windows. Each window is considered as an instance for feature extraction, from which we have extracted both the OFS and VFS features.

As the feature set becomes large after adding the VFS, we applied the well-known Correlation Feature Selection (CFS) algorithm [55] to reduce the feature set to the most informative features and discarding the redundant and less informative features. Table 4 shows the reduced feature sets when applying the CFS algorithm on accelerometer and KEH data for both hand and waist placements. For the accelerometer data, the number of features is reduced from 83 to 22 in the hand placement case, and 16 in the waist placement case. For the KEH data, the number of features is reduced from 26 to 10 in the hand placement case, and 9 in the waist placement case. As will be shown later, the reduced feature set is as effective as the original large set in detecting human activities.

An interesting outcome of the feature reduction exercise is that it identified only two features, PktPk and PktPkDiff, for the Hand placement and PktPk and maxPk for the Waist placement from the 7 features in the VFS. This means that these are the most important vibration features for HARKE. In the following section, we will evaluate the impact of the vibration features on the performance of HARKE.
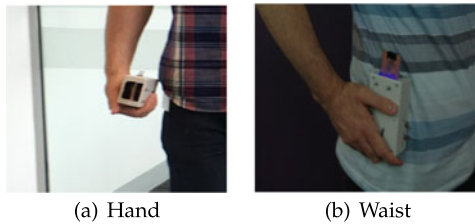
6.5 Performance Evaluation

In this section, we analyse HARKE performance based on the practical KEH data and we relate the results to those
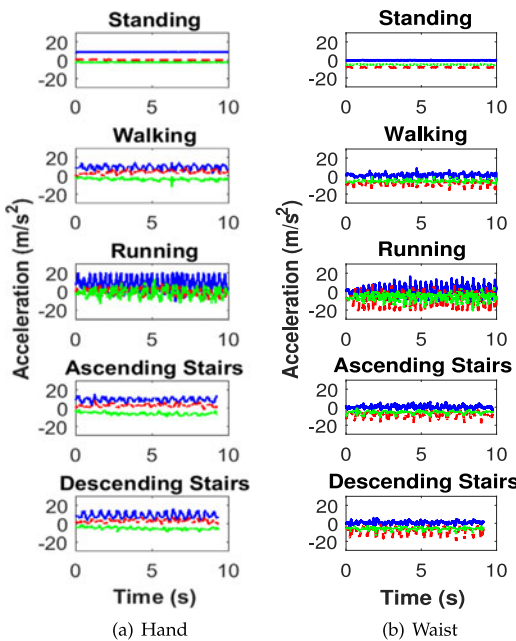

Fig. 10. The accelerometer patterns of the five activities for two placements: (a) Hand and (b) Waist.
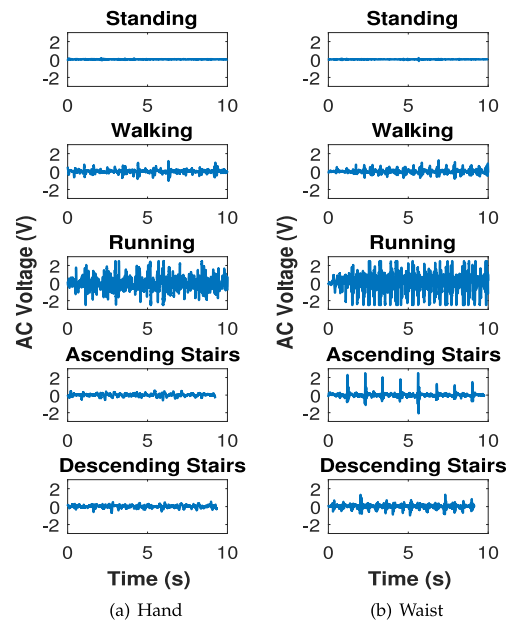

Fig. 11. The KEH patterns of the five activities for two placements: (a) Handx and (b) Waist.

TABLE 3
The Vibration Feature Set (VFS) Used to Quantify
the Vibration Level in Both Accelerometer and KEH Data

Feature	Abbreviation	Description
Root Mean Square	RMS	The square root of the arithmetic mean of the squares of the values. The RMS is a measurement of the effective energy content in a the signal.
Peak-to-Peak	PktPk	The difference between the maximum peak value and the minimum peak value. It indicates the maximum excursion of the signal.
Peak-to-Peak Difference	PktPkDiff	The difference between the maximum difference between peak values and the minimum difference between peak values of the sinusoidal wave. It indicates the maximum excursion of the time periods.
mean Peak	meanPk	The mean value of the differences between all the peak values. It quantifies the average variation level of the values of the signal.
mean Peak Distance	meanDisPk	The mean value of the differences between the all the distances (time periods) between peak values. It quantifies the average variation level of the time periods of the signal.
maximum Peak	maxPk	The maximum value of the differences between all the peak values. It quantifies the maximum variation level of the time periods of the signal.
maximum Peak Distance	maxDisPk	The maximum value of the differences between all the distances (time periods) between peak values. It quantifies the maximum variation level of the time periods of the signal.

TABLE 4
The Resulting Feature Sets of the CFS Algorithm

HARAC		HARKE	
Hand Placement	Waist Placement	Hand Placement	Waist Placement
varZ	CVY	absArea	absMean
stdZ	VarY	var	absArea
IQRZ	FDEnergyY	IQR	RMS
PktPkDiffY	IQRY	Q3	Q1
CVX	Q3Y	min	range
meanDismPkX	Q1Y	Q1	min
PktPkZ	MaxY	range	Q3
MaxPeaksY	PktPkDiffY	PktPk	PktPk
PktPkDiffX	meanDisPksY	max	maxPk
RMSX	stdX	PktPkDiff	
MaxPeaksX	FDEnergyX		
IQRY	RMSX		
MinZ	DFRatioX		
meanDisPkY	skewY		
meanDisPkZ	skewZ		
Q1Z	CorrXZ		
CVY			
totalMA			
absArea			
CorrXY			
MinY			
SkewX			

TABLE 5
HARKE Performance

	with OFS		with OFS+VFS		with CFS	
Classifier	Hand	Waist	Hand	Waist	Hand	Waist
NN	**70.21**	**83.51**	80.11	87.36	80.19	86.08
DT	76.34	79.27	79.76	80.34	74.93	77.89
SVM	72.89	75.74	72.89	79.66	71.72	72.41
NB	70.58	69.15	70.58	70.90	70.80	73.63

the OFS yields an improvement in the performance. Then, we investigate whether the use of the CFS reduced feature set, shown in Table 4, affects the performance of activity recognition. We also examine the impact of body placements of the wearable, and the similarity of the activities on the recognition accuracy. Next, we compare the activity recognition accuracies that are obtained from the model-based power data against those obtained using the ground truth hardware data. Finally, we compare the performance of HARKE to the conventional accelerometer-based human activity recognition, HARAC.

In order to analyse the performance of HARKE, we train and test the classifiers using 10-fold cross validation [56], which divides the entire dataset into 10 sets with 9 of them used for training and the remaining one for testing. This process is repeated 10 times and the average of the 10 repetitions is reported. Table 5 shows the recognition accuracies (%) of HARKE using the previously mentioned classifiers when the OFS, the combined set of OFS and VFS (OFS+VFS), and the CFS reduced feature set (CFS) are used, for both hand and waist placement cases. For each case, the highest accuracy obtained is shown in bold. We can see that the nearest neighbor (NN) classifier achieves the highest accuracies in most cases.

6.5.1   Impact of Vibration Features
In this section, we explore if adding the VFS, shown in Table 3, to the OFS yields an improvement in the performance. Table 5 demonstrates that adding VFS improves the accuracy of HARKE significantly as compared to the case when OFS is used and no vibration features are used. VFS improves HARKE accuracies noticeably from 70.21 to 80.11 percent for the hand placement case and 83.51 to 87.36 percent in the waist placement case with NN classifier. This is because the VFS contains features which are typically used to quantify the severity of the vibration through peak analysis [54]. This helps us distinguish the activities more accurately and hence improve the performance of HARKE.

6.5.2   Impact of Feature Reduction
Earlier in this section, we showed that the CFS algorithm has significantly reduced the number of features for HARKE from 26 features to only 10 and 9, as shown in Table 4, for the hand and the waist placements, respectively. In this section, we investigate whether the use of the CFS reduced feature set affects the activity recognition performance of HARKE. Table 5 shows the accuracies (%) of HARKE when the CFS reduced feature set (CFS) is used for both hand and waist placements. We find that NN is the most effective classifier with CFS. These results show that the CFS reduced feature set is as effective as the combined set (OFS+VFS) in detecting human activities when the NN classifier is used. Using only 10 and 9 time domain features

obtained from the publicly available motion data obtained through theoretical modeling. First, we show the performance of HARKE when the OFS (shown in Table 1) is used. Next, we explore if adding the VFS (shown in Table 3) to

TABLE 6
The Confusion Matrix of HARKE for **Hand** Placement Using the CFS Reduced Feature Set When the NN Classifier is Used

| | | Classified as | | | | | TP Rate |
		WALK	RUN	STAND	SU	SD	
	WALK	48	0	0	12	4	0.75
	RUN	0	54	0	0	0	1
	STAND	0	0	73	0	0	1
Activity	SU	17	0	1	18	3	0.46
	SD	10	0	0	6	16	0.5

TABLE 7
The Confusion Matrix of HARKE for **Waist** Placement Using the CFS Reduced Feature Set When the NN Classifier is Used

| | | Classified as | | | | | TP Rate |
		WALK	RUN	STAND	SU	SD	
	WALK	61	0	0	2	3	0.92
	RUN	0	66	0	0	0	1
	STAND	0	0	72	0	0	1
Activity	SU	5	0	1	29	7	0.69
	SD	9	3	0	9	18	0.46

(shown in Table 4) with NN classifier, HARKE achieves 80.19 and 86.08 percent accuracy for hand and waist placements, respectively.

6.5.3 Impact of Body Position

The performance of HARKE is highly affected by the position where the device is placed on the user's body. Table 5 shows that the waist placement gives higher classification accuracies than hand placement. This is consistent with the observation in the previous section, which showed that torso provides better performance compared to arm and leg placements. This is quite meaningful because when the device is closer to the central part of the body, it can sense the activity more accurately. So depending on the accuracy requirement of the application, the device placement on the human body has to be chosen carefully. For example, health specific applications might require the device to be placed near the central part of the body to achieve the required accuracy [57].

6.5.4 Impact of Similar Activities

Recall that in Section 5.4, we observed that similar activities, such as going up and down the stairs, are difficult to detect with KEH power traces estimated from a public motion dataset. To investigate whether this is also the case with the practical KEH data, we examine the confusion matrices of HARKE for hand and waist placements in Tables 6 and 7, respectively. Standing (STAND) and running (RUN) activities are identified with very high (100 percent) accuracy, but the true positive (TP) rate is significantly lower for WALK, SU, and SD. This is due to the fact that these activities are quite similar in behaviour as the users periodically move their legs for either walking, going up or down stairs. This means that HARKE could be used reliably as long as the activities are not too similar, but its performance would start to deteriorate as soon as very similar activities are added to the target set. The confusion between similar activities is slightly reduced for waist placement as the attachment of the
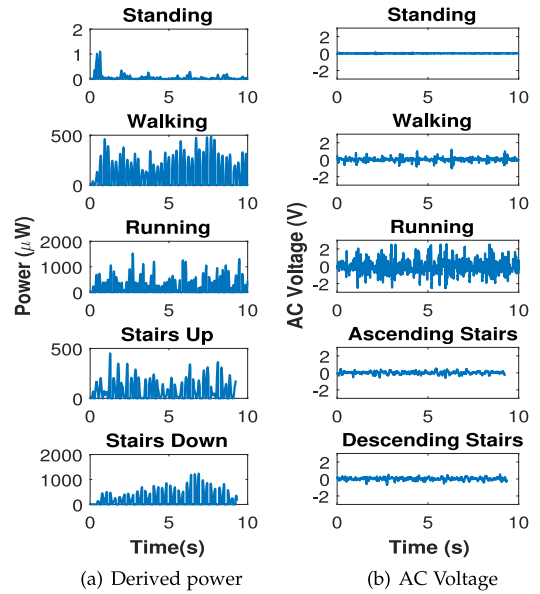

Fig. 12. Derived KEH power versus hardware AC voltage.

device to the central part of the body helps in sensing and identifying those similar activities more accurately. This is also confirmed in Section 5.4 with the public dataset where HARKE achieves above 0.9 TP rate for all activities including similar ones such as SU and SD for Torso position.

6.5.5 Model versus Hardware

As our hardware records both accelerometer and ground truth AC voltage data, we have an opportunity to assess the validity of the mass-spring model used in our earlier analysis for the publicly available accelerometer data sets. Let us point out that our hardware was designed to collect only the AC voltage data. We have not built the complete circuit to convert the AC voltage to DC power, nor any power optimization was used for the circuit or piezoelectric transducer. As such, a direct match between the theoretical model and the ground truth data, i.e., the raw power data, cannot be expected. It would be more appropriate to compare the activity recognition accuracies that are obtained from the model-based power data against those obtained using the ground truth AC voltage data.

We first compare the model-derived power data against the ground truth AC voltage data in Fig. 12, which shows that both data sets capture variations due to the different activities that generate them. Then we compare the activity recognition accuracies based on model-derived data and ground truth AC voltage data in Fig. 13, which compares results from the classifiers that produce the best results for these two data sets (i.e., DT for model-based power data and NN for ground truth AC voltage). As can be seen from this figure, the activity recognition accuracies obtained with ground truth AC voltage are very similar to the ones obtained with power data derived from the accelerometer traces using the mass-spring model. Additionally, the fundamental conclusions about human activity recognition accuracies, e.g., the waist placement can give better accuracy over the hand placement, can also be accurately obtained using the model. We can therefore conclude that the mass-spring model can be reliably used for KEH-based activity recognition studies when only the accelerometer data are available.
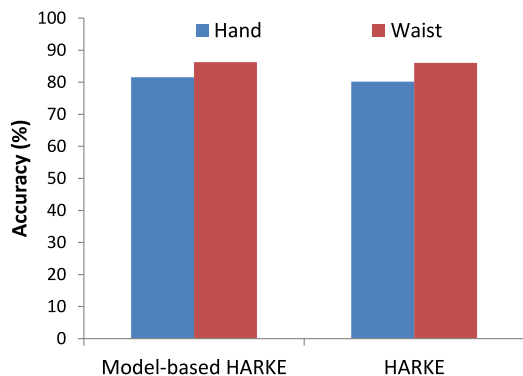
Fig. 13. Performance comparison of model-based evaluation using DT classifier and hardware-based evaluation using NN.

6.5.6 HARKE versus HARAC

In this section, we compare the performance of HARKE (as shown in Table 5) with HARAC (as summarized in Table 8). We make the following observations. First, the nearest neighbor (NN) classifier appear to achieve the highest accuracies for both HARKE and HARAC in most cases. Second, for both methods, CFS reduces the number of features significantly without sacrificing activity recognition accuracies. Third, the use of vibration features (i.e., the VFS) has no noticeable impact on the performance of HARAC, whereas it obtains significant improvement for HARKE.

A comparison between Tables 5 and 8 also confirms the expected *accuracy gap* between HARKE and HARAC, which we already observed in Section 5.4 using the public data set. This time, HARKE accuracies are lower than those of HARAC by 14.82 and 13.07 percent for hand and waist placements, respectively. This is clearly due to the multi-dimensional (three-axial) measurements of the accelerometer signal. The accelerometer provides X, Y, and Z components of acceleration (shown in Fig. 10), whereas KEH is a single-axial AC voltage signal (shown in Fig. 11). A 3-axial accelerometer is fundamentally advantageous in separating very similar human activities, such as going up and down the stairs due to the multi-dimensional measurement of the motion, hence achieving very high performance. Fortunately, as observed in Section 5.4, the accuracy gap between HARKE and HARAC can be reduced significantly by placing the device closer to the chest (torso placement).

In the next section, we conduct a detailed power measurement study to analyse and quantify the power saving opportunity for HARKE.

7 POWER MEASUREMENT

The key motivation of our proposed HARKE architecture is energy saving by eliminating the need for powering an accelerometer to sense human activity. Unlike the conventional accelerometer-based HARAC approach, HARKE samples only a transducer that remains active all the time without requiring any power supply. An earlier measurement study tested the power consumption of six commonly used capacitive accelerometers when a 3.3v power supply and a 50 HZ sampling rate were used. The results showed that accelerometers consume hundreds of microwatts at only 50 Hz sampling rate which could be saved by HARKE. In fact, the exact amount of power that can be saved by HARKE will depend on the design configurations of actual systems which may have different kind of accelerometer and different ways of

TABLE 8
HARAC Performance

Classifier	with OFS		with OFS+VFS		with CFS	
	Hand	Waist	Hand	Waist	Hand	Waist
NN	**95.44**	**99.64**	**95.81**	**99.64**	**95.01**	**99.15**
DT	87.02	90.59	88.19	91.27	86.33	93.26
SVM	90.43	96.86	88.89	98.24	88.38	87.51
NB	84.69	88.44	85.44	88.09	88.54	91.51

sampling it. However, fundamentally, significant amount of power can be saved by not having to power up an accelerometer for each sensor sampling. Moreover, HARAC generates three times of data samples (3-axial accelerometer) but HARKE generates a single axis data trace to be transmitted which can also save significant power of data transmission.

In this section, we carry out a detailed measurement study to quantify the power savings of HARKE compared to HARAC using a typical configuration of today's energy efficient wearable devices. The main variables measured for HARKE and HARAC are the length of the sampling interval, the average power consumption during the interval for each sampling event, and the average power consumption of data transmission.

7.1 Measurement Setup

We use an off-the-shelf Texas Instruments SensorTag [58] as the target measurement device, which includes an ultra-low power ARM Cortex-M3 MCU specifically designed for today's energy-efficient wearable devices, such as FitBit fitness trackers [59], [60]. The SensorTag is embedded with the CC2650 microcontroller (MCU) [61], which provides ultra-low power consumption, and the InvenSense MPU9250 9-axis motion sensor. Our SensorTag is running with the Contiki 2.6 operating system [62] which utilizes the power saving features of the CC2650. The processing event running on Contiki has been programmed to sample either the 3-axial acceleration signal from the MPU9250 motion sensor, or the voltage signal of the supply power source. The Contiki OS has been programmed to put the MCU into deep-sleep mode when there are no sampling events in the OS event queue. When a sampling event occurs, the MCU is awakened from deep-sleep mode by software interrupts.

Fig. 14a shows the energy measurement setup. The SensorTag (shown at the top part) is connected with the oscilloscope (shown at the bottom). We use the Agilent DSO3202A oscilloscope to capture both the current consumption and time duration for each acceleration and voltage sampling event. The SensorTag is first connected with a 10Ω resistor in series, and powered by the 3V coin battery. Then, the oscilloscope probe is connected across the resistor to measure the voltage.

In the remaining of this section, we first measure the power consumption due to data *sampling*, which will be followed by the analysis of *transmission* power consumption. Finally, we will analyze the *overall* system power consumption considering both *sampling* and *transmission* power consumptions.

7.2 Power Consumption for Sampling

Separate measurements are done to quantify the sampling power consumptions for HARAC and HARKE.

7.2.1 HARAC

Accelerometers generally come in two different types–digital and analog. Digital accelerometers produce acceleration in

(a) Measurement setup.   (b) Profiling of accelerometer sampling.   (c) Profiling of KEH (voltage) sampling.
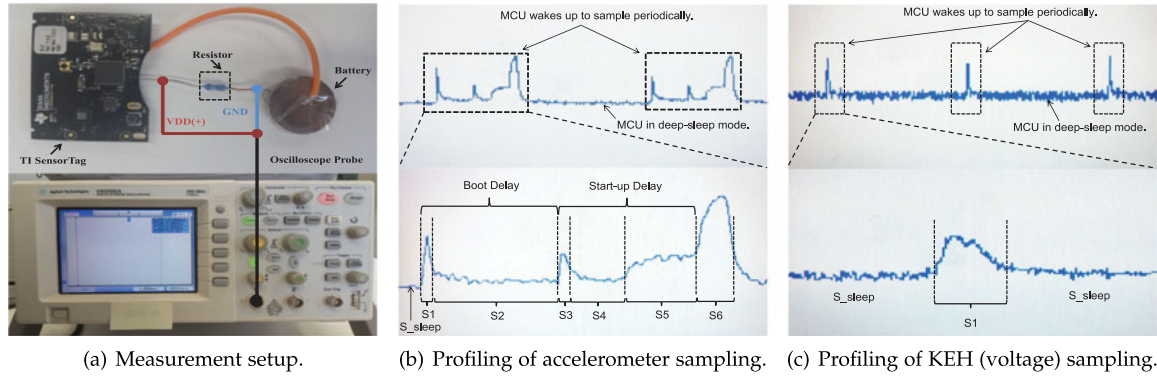
Fig. 14. The experimental setup for the power measurement and the results for both accelerometer and KEH sampling.

digital format, which can be read and used directly by activity classification process. However, an I^2C bus has to be powered separately to read the data from the digital accelerometer. Analog accelerometers, on the other hand, produce analog data, which can be read directly using an analog-to-digital converter (ADC) instead of powering an I^2C bus. Therefore sampling analog accelerometers could avoid power consumption related to the I^2C bus, but at the expense of some processing cost to convert analog signals into digital. While it is not immediately obvious whether digital accelerometer sampling would be less or more power consuming relative to the analog counterpart, an earlier measurement study [63] has confirmed that digital accelerometer is more power efficient than the comparable analog ones from the same manufacturers. Based on this finding, we choose to use digital accelerometers for our study.

The SensorTag includes a 9-axis digital MPU92507 motion sensor combining a 3-axis gyroscope and a 3-axis compass along with a 3-axis accelerometer. During the power measurements, we only enable the accelerometer and leave all the other sensors turned off. The digital accelerometer is sampled at 25Hz using the I^2C bus embedded in the SensorTag.

Fig. 14b shows the power measurement profile of the accelerometer sampling. It shows the periodical sampling of the accelerometer (in the top part of the figure) and the details for each sampling event (in the bottom). The MCU automatically goes to the deep-sleep mode between each sampling event to reduce the overall system energy consumption. As observed from the figure, the accelerometer sampling event is divided into six states (S1 - S6).

At the beginning of each event, the software timer interrupts the MCU from the deep-sleep mode (S_sleep), so that the MCU wakes up to boot the accelerometer and then goes back to sleep (S1). The accelerometer is powering up during S2 when the MCU sleeps. Then, after one software clock tick (7.8 ms in Contiki OS), the MCU wakes up again to initialize the accelerometer, and then goes back to sleep (S3). The accelerometer completes initialization and becomes active after S5. Then, MCU wakes up again to read the accelerometer sample during S6, and goes back to deep-sleep mode after finishing. The details of the power consumption and time duration for all the states in the accelerometer sampling event are stated in Table 9. Based on these measurements, we find that the length of each accelerometer sampling is 17.2 ms in total and 322 μW of power is consumed on average during this interval. This means that for each accelerometer sampling, the system consumes $17.2 \times 322 = 5.5$ μJ of energy.

7.2.2 HARKE

In this section, we investigate the power consumption in sampling the voltage signal from the power source. The signal can be either the voltage coming out from the energy harvester (transducer) directly, or the voltage of the battery powered by the energy harvesting transducer. To ensure stable power supply, in our measurement, the MCU is programmed to periodically sample the supply voltage coming out from the lithium coin battery with 25 Hz sampling rate. The MCU reads voltage signal through ADC. Fig. 14c shows that similar to the accelerometer, the MCU goes back to deep-sleep mode after each sampling event. However, the sampling takes only 0.6 ms with an average power consumption of 480 μW, which means that only $0.6 \times 480 = 0.3$ μJ is consumed for each sampling in the HARKE system (details of the power consumption and time duration for all the states in the voltage sampling event are stated in Table 10).

7.2.3 HARAC versus HARKE for Different Sampling Rates

Now, let us compare the sampling-related power consumption for HARAC and HARKE for different sampling rates. For a duty-cycled system, the sampling power consumption, P, can be obtained as

$$P = \begin{cases} \frac{t \times n}{1000} P_{sample} + \left(1 - \frac{t \times n}{1000}\right) P_{sleep} & \text{if } 0 \leq n \leq \frac{1000}{t}, \\ P_{sample} & \text{if } \frac{1000}{t} < n. \end{cases} \quad (11)$$

TABLE 9
States of Accelerometer Sampling, Which Takes 17.2 ms in Total and Consumes 322 μW on Average during this Interval

State	Duration (ms)	Power Consumption (μW)	Description
S1	0.6	480	MCU wakes up to boot accelerometer.
S2	7.2	72	MCU goes back to sleep when accelerometer starts booting.
S3	0.6	480	MCU wakes up to initiate accelerometer.
S4	3.2	72	MCU goes back to sleep when accelerometer starts initializing.
S5	4	480	Accelerometer is turning on.
S6	1.6	1440	MCU wakes up to sample accelerometer signal.
S_sleep	null	6	MCU in deep-sleep mode; Accelerometer is turned-off.

TABLE 10
States of Voltage Sampling, Which Takes 0.6 ms in Total and
Consumes 480 μW on Average during this Interval

State	Duration (ms)	Power Consumption (μW)	Description
S1	0.6	480	MCU wakes up to sample voltage signal.
S_sleep	null	6	MCU in deep-sleep mode.

where, P_{sample} is the power consumption of the system during each sampling event, P_{sleep} is the power consumption when the MCU is in deep-sleep mode, n is the sampling frequency in Hz, and t is the interval length of a sampling event in units of ms. Fig. 15 compares the power consumption of HARKE against HARAC for the range of sampling frequencies applicable for human activity recognition. HARKE exhibits huge power saving as the required sampling rate starts to increase. Considering a very modest sampling rate of 10 Hz, which is the lowest reported sampling rate for HAR, based on our measurements, HARAC consumes 60.35 μW while HARKE consumes only 8.84 μW in data sampling.

Now let us consider an example of a typical wearable system that samples at a rate of 10 Hz, but accumulates sampled data for every 10 seconds before transmitting them to the data centre in a batch. The sampling power consumption for each 10-sec cycle is therefore 603.5 μJ and 88.4 μJ for HARAC and HARKE, respectively. In the next section, we are going to evaluate the power consumption due to the transmission of these sampled data.

7.3 Power Consumption for Data Transmission

To account for the power consumption due to transmissions, we conduct power measurement of Bluetooth Low Energy (BLE) using the embedded CC2650 wireless MCU in the SensorTag. This BLE has a data rate of 1 Mbps and it retransmits every packet over three different channels for improved reliability. We programmed the Contiki OS to wake-up the CC2650 MCU periodically to transmit a BLE packet of maximum length (i.e., 28 bytes of payload plus 19 bytes of header). The measurement results indicate that BLE transmission consumes 2.72 mW on average, which applies to both HARKE and HARAC. Note, however, that the transmission *energy* consumption will eventually depend on the duration it takes for the BLE to complete the transmission of all data sampled during the last 10-sec. Given the use of the 3-axial accelerometer, HARAC is expected to produce three times as much data as compared to HARKE, which means the BLE transmissions would be equally longer and the transmission-related energy consumption would be equally higher.

With 3-axial accelerometer, HARAC generates 300 acceleration samples (at 10 Hz) in 10 seconds, which results in 600 bytes of data to be transmitted in total (i.e., 2 bytes for each acceleration sample). According to our measurements, it takes 106.11 ms for HARAC to transmit these 600 byte over BLE, including the BLE packet overhead and the time spent due to retransmissions on separate channels. HARAC therefore consumes $2.72 \ mW \times 106.11 \ ms = 288.62 \ \mu$J of transmission energy for every 10-sec cycle of sampling and data transmission.

HARKE, on the other hand, generates only 100 voltage samples (at 10 Hz) within 10 seconds, which results in 200 bytes of data to be transmitted in total (2 bytes for each of
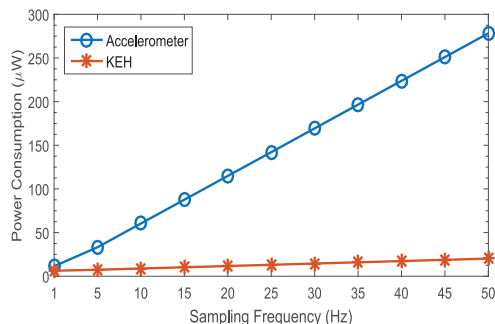

Fig. 15. Power consumption as a function of sampling frequency.

the 12-bits ADC voltage reading). According to our measurements, it takes 35.37 ms to transmit these bytes. This results in the consumption of $2.72 \ mW \times 35.37 \ ms = 96.21 \ \mu$J of transmission energy for HARKE.

7.4 Overall System Power Consumption

The overall energy consumption of a wearable health tracker mainly comes from two different parts: data sampling and data transmission. For the example wearable system, the overall system energy consumption is therefore obtained as $603.5 + 288.62 = 892.12 \ \mu$J and $88.4 + 96.21 = 184.61 \ \mu$J for HARAC and HARKE, respectively. This indicates that HARKE can save approximately 79.31 percent of the overall system energy consumption as compared to HARAC. Note that although we used a 10-sec cycle as an example, this amount of power saving is valid irrespective of the cycle length.

8 Conclusion and Future Directions

In this paper we have proposed a novel method of human activity recognition, called HARKE, directly from the kinetic energy harvesting patterns without using any accelerometer. With detailed power measurements, we have demonstrated that HARKE can potentially reduce system power consumption by 79 percent compared to existing accelerometer-based activity detection systems. Our study has revealed that HARKE can detect daily activities with 80 to 95 percent accuracy depending on the activities and the placement (location) of the wearable device on the human body. These accuracies are within 4 percent of existing accelerometer-based methods if the wearable device is placed close to the chest and within 15 percent when the device is attached to the hand or arm. Therefore, HARKE can be readily used in chest-worn devices for applications that can tolerate slightly lower accuracies.

The activities we have evaluated exhibit significant repetitiveness. It is therefore expected that our results will be valid for many other activities, such as gym activities, that are also repetitive. However, there exist more sophisticated activities, such as eating, drinking, cooking, etc., which are not as repetitive as walking and running. Detecting such complex activities are much more challenging than the repetitive ones.

While the current work clearly demonstrates the usefulness of HARKE in detecting many basic activities of daily living, a future direction will be to investigate the potential of detecting more complex activities, possibly using wrist-worn devices, similar to [3], [4]. To this end, we can explore some of the recent discoveries in energy harvesting research, such as multi-axial energy harvesters [64] that harvest energy from multiple dimensions and could potentially

provide much richer information about human motion compared to the existing harvesters. Similarly, future self-tunable energy harvesters [65] will provide opportunity to always keep the resonance of the harvester tuned to the current human activity, offering better signals for activity detection. Finally, we plan to explore how to leverage the recent advancements in machine learning algorithms, such as Deep Learning constructs [3], to detect complex activities from crude energy harvesting signals with higher accuracy.

ACKNOWLEDGMENTS

REFERENCES

[1] O. Chipara, C. Lu, T. C. Bailey, and G.-C. Roman, "Reliable clinical monitoring using wireless sensor networks: Experiences in a step-down hospital unit," in *Proc. 8th ACM Conf. Embedded Netw. Sensor Syst.*, 2010, pp. 155–168.

[2] F. Albinali, S. Intille, W. Haskell, and M. Rosenberger, "Using wearable activity type detection to improve physical activity energy expenditure estimation," in *Proc. 12th ACM Int. Conf. Ubiquitous Comput.*, 2010, pp. 311–320.

[3] P. Vepakomma, D. De, S. K. Das, and S. Bhansali, "A-wristocracy: Deep learning on wrist-worn sensing for recognition of user complex activities," in *Proc. IEEE 12th Int. Conf. Wearable Implantable Body Sensor Netw.*, Jun. 2015, pp. 1–6.

[4] D. De, P. Bharti, S. K. Das, and S. Chellappan, "Multimodal wearable sensing for fine-grained activity recognition in healthcare," *IEEE Internet Comput.*, vol. 19, no. 5, pp. 26–35, Sep. 2015.

[5] U. Maurer, A. Smailagic, D. P. Siewiorek, and M. Deisher, "Activity recognition and monitoring using multiple sensors on different body positions," in *Proc. Int. Workshop Wearable Implantable Body Sensor Netw.*, Apr. 2006, Art. no. 116.

[6] B. Tessendorf, et al., "Recognitio vbvbc/bn of hearing needs from body and eye movements to improve hearing instruments," in *Proc. Int. Conf. Pervasive Comput.*, 2011, pp. 314–331.

[7] K. Altun and B. Barshan, "Pedestrian dead reckoning employing simultaneous activity recognition cues," *Meas. Sci. Technol.*, vol. 23, no. 2, pp. 1–20, Feb. 2012.

[8] M. Hassan, "A performance model of pedestrian dead reckoning with activity-based location updates," in *Proc. IEEE Int. Conf. Netw.*, 12–14 Dec. 2012, pp. 64–69.

[9] S. Khalifa, M. Hassan, and A. Seneviratne, "Feature selection for floor-changing activity recognition in multi-floor pedestrian navigation," in *Proc. 7th Int. Conf. Mobile Comput. Ubiquitous Netw.*, 2014, pp. 1–6.

[10] S. Khalifa, M. Hassan, and A. Seneviratne, "Adaptive pedestrian activity classification for indoor dead reckoning systems," in *Proc. Int. Conf. Indoor Positioning Indoor Navigation*, Oct. 2013, pp. 1–7.

[11] P. Mitcheson, E. Yeatman, G. Rao, A. Holmes, and T. Green, "Energy harvesting from human and machine motion for wireless electronic devices," *Proc. IEEE*, vol. 96, no. 9, pp. 1457–1486, Sep. 2008.

[12] J. Yun, S. Patel, M. Reynolds, and G. Abowd, "A quantitative investigation of inertial power harvesting for human-powered devices," in *Proc. 10th Int. Conf. Ubiquitous Comput.*, 21–24 Sep. 2008, pp. 74–83.

[13] J. Yun, S. N. Patel, M. S. Reynolds, and G. D. Abowd, "Design and performance of an optimal inertial power harvester for human-powered devices," *IEEE Trans. Mobile Comput*, vol. 10, no. 5, pp. 669–683, May 2011.

[14] M. Gorlatova, J. Sarik, G. Grebla, M. Cong, I. Kymissis, and G. Zussman, "Movers and shakers: Kinetic energy harvesting for the internet of things," *ACM SIGMETRICS Perform. Eval. Rev.*, vol. 42, no. 1, pp. 407–419, Jun. 2014.

[15] Z. Yan, V. Subbaraju, D. Chakraborty, A. Misra, and K. Aberer, "Energy-efficient continuous activity recognition on mobile phones: An activity-adaptive approach," in *Proc. 16th Annu. Int. Symp. Wearable Comput.*, 18–22 Jun. 2012, pp. 17–24.

[16] L. Bao and S. S. Intille, "Activity recognition from user-annotated acceleration data," *Pervasive Comput.*, vol. 3001, pp. 1–17, 2004.

[17] J. Baek, G. Lee, W. Park, and B.-J. Yun, "Accelerometer signal processing for user activity detection," in *Knowledge-Based Intelligent Information and Engineering Systems*. Berlin, Heidelberg: Springer, 2004, vol. 3215, pp. 610–617.

[18] K. Altun, B. Barshan, and O. Tunçel, "Comparative study on classifying human activities with miniature inertial and magnetic sensors," *Pattern Recog.*, vol. 43, no. 10, pp. 3605–3620, 2010.

[19] J. R. Kwapisz, G. M. Weiss, and S. A. Moore, "Activity recognition using cell phone accelerometers," *ACM SIGKDD Explorations Newslett.*, vol. 12, no. 2, pp. 74–82, 2010.

[20] A. Parnandi, et al., "Coarse in-building localization with smartphones," in *Mobile Computing, Applications, and Services*. Berlin, Heidelberg: Springer, 2010, vol. 35, pp. 343–354.

[21] M. Ayu, T. Mantoro, A. Matin, and S. Basamh, "Recognizing user activity based on accelerometer data from a mobile phone," in *Proc. IEEE Int. Symp. Comput. Inf.*, 20–23 Mar. 2011, pp. 617–621.

[22] S. Khalifa, M. Hassan, and A. Seneviratne, "Pervasive self-powered human activity recognition without the accelerometer," in *Proc. Int. Conf. Pervasive Comput. Commun.*, Mar. 2015, pp. 79–86.

[23] K. Altun, B. Barshan, and O. Tunçel, "Comparative study on classifying human activities with miniature inertial and magnetic sensors," *Pattern Recog.*, vol. 43, no. 10, pp. 3605–3620, 2010.

[24] L. Chen, J. Hoey, C. D. Nugent, D. J. Cook, and Z. Yu, "Sensor-based activity recognition," *IEEE Trans. Syst. Man Cybern. Part C Appl. Rev.*, vol. 42, no. 6, pp. 790–808, Nov. 2012.

[25] R. Bodor, B. Jackson, N. Papanikolopoulos, and H. Tracking, "Vision-based human tracking and activity recognition," in *Proc. 11th Mediterranean Conf. Control Autom.*, 2003, pp. 18–20.

[26] R. Poppe, "A survey on vision-based human action recognition," *Image Vis. Comput.*, vol. 28, no. 6, pp. 976–990, 2010.

[27] S. Wang and G. Zhou, "A review on radio based activity recognition," *Dig. Commun. Netw.*, vol. 1, no. 1, pp. 20–29, 2015.

[28] L. Yang, Y. Chen, X.-Y. Li, C. Xiao, M. Li, and Y. Liu, "Tagoram: Real-time tracking of mobile RFID tags to high precision using cots devices," in *Proc. 20th Annu. Int. Conf. Mobile Comput. Netw.*, 2014, pp. 237–248.

[29] M. Philipose, et al., "Inferring activities from interactions with objects," *IEEE Pervasive Comput.*, vol. 3, no. 4, pp. 50–57, Oct.–Dec. 2004.

[30] L. Shangguan, Z. Zhou, X. Zheng, L. Yang, Y. Liu, and J. Han, "ShopMiner: Mining customer shopping behavior in physical clothing stores with cots RFID devices," in *Proc. 13th ACM Conf. Embedded Netw. Sensor Syst.*, 2015, pp. 113–125.

[31] H. Ding, et al., "FEMO: A platform for free-weight exercise monitoring with RFIDs," in *Proc. 13th ACM Conf. Embedded Netw. Sensor Syst.*, 2015, pp. 141–154.

[32] B. Kellogg, V. Talla, and S. Gollakota, "Bringing gesture recognition to all devices," in *Proc. 11th USENIX Conf. Netw. Syst. Des. Implementation*, 2014, pp. 303–316.

[33] M. Philipose, J. R. Smith, B. Jiang, A. Mamishev, S. Roy, and K. Sundara-Rajan, "Battery-free wireless identification and sensing," *IEEE Pervasive Comput.*, vol. 4, no. 1, pp. 37–45, Jan. 2005.

[34] A. Yurtman and B. Barshan, "Human activity recognition using tag-based radio frequency localization," *Appl. Artif. Intell.*, vol. 30, no. 2, pp. 153–179, Feb. 2016.

[35] O. Lara and M. Labrador, "A survey on human activity recognition using wearable sensors," *IEEE Commun. Surveys Tutorials*, vol. 15, no. 3, pp. 1192–1209, Mar. 2013.

[36] S. Seneviratne, et al., "A survey of wearable devices and challenges," *IEEE Commun. Surveys Tutorials*, vol. PP, no. 99, p. 1, 2017.

[37] P. Zappi, et al., "Activity recognition from on-body sensors: Accuracy-power trade-off by dynamic sensor selection," in *Proc. Eur. Conf. Wireless Sensor Netw.*, Feb. 2008, pp. 17–33.

[38] Y. Wang, et al., "A framework of energy efficient mobile sensing for automatic user state recognition," in *Proc. 7th Int. Conf. Mobile Syst. Appl. Services*, 2009, pp. 179–192.

[39] D. Gordon, J. Czerny, T. Miyaki, and M. Beigl, "Energy-efficient activity recognition using prediction," in *Proc. 16th Int. Symp. Wearable Comput.*, 2012, pp. 29–36.

[40] A. Krause, et al., "Trading off prediction accuracy and power consumption for context-aware wearable computing," in *Proc. IEEE Int. Symp. Wearable Comput.*, 2005, pp. 20–26.

[41] Z. Yan, V. Subbaraju, D. Chakraborty, A. Misra, and K. Aberer, "Energy-efficient continuous activity recognition on mobile phones: An activity-adaptive approach," in *Proc. 16th Annu. Int. Symp. Wearable Comput.*, 18–22 June 2012, pp. 17–24.

[42] X. Qi, M. Keally, G. Zhou, Y. Li, and Z. Ren, "AdaSense: Adapting sampling rates for activity recognition in body sensor networks," in *Proc. IEEE 19th Real-Time Embedded Technol. Appl. Symp.*, 2013, 163–172.

[43] R. Vullers, R. van Schaijk, I. Doms, C. V. Hoof, and R. Mertens, "Micropower energy harvesting," *Solid-State Electron.*, vol. 53, no. 7, pp. 684–693, 2009.

[44] S. Khalifa, M. Hassan, A. Seneviratne, and S. K. Das, "Energy-harvesting wearables for activity-aware services," *IEEE Internet Comput.*, vol. 19, no. 5, pp. 8–16, Sep./Oct. 2015.

[45] C.-C. Yang and Y.-L. Hsu, "A review of accelerometry-based wearable motion detectors for physical activity monitoring," *Sensors*, vol. 10, no. 8, pp. 7772–7788, 2010.

[46] Accelerometer basics. [Online]. Available: https://learn.sparkfun.com/tutorials/accelerometer-basics, Accessed on: 4 Aug. 2016.

[47] Y. Rao, S. Cheng, and D. P. Arnold, "An energy harvesting system for passively generating power from human activities," *J. Micromechanics Microengineering*, vol. 23, no. 11, p. 114012, 2013.

[48] E. Lefeuvre, A. Badel, C. Richard, L. Petit, and D. Guyomar, "A comparison between several vibration-powered piezoelectric generators for standalone systems," *Sensors Actuators*, vol. 126, no. 2, pp. 405–416, 2006.

[49] S. Khalifa, "Inertial Kinetic Energy Harvesting Model." [Online]. Available: http://www.mathworks.com/matlabcentral/fileexchange/53585-inertial-kinetic-energy-harvesting-model, Accessed on: 17 Oct. 2017.

[50] J. R. Quinlan, *C4.5: Programs for Machine Learning*. San Francisco, CA, USA: Morgan Kaufmann Publishers, 1993.

[51] D. W. Aha, D. Kibler, and M. K. Albert, "Instance-based learning algorithms," *Mach. Learn.*, vol. 6, no. 1, pp. 37–66, 1991.

[52] C.-C. Chang and C.-J. Lin, "LIBSVM - a library for support vector machines," The Weka classifier works with version 2.82 of LIBSVM, 2001. [Online]. Available: http://www.csie.ntu.edu.tw/cjlin/libsvm/

[53] WEKA Software. [Online]. Available: http://www.cs.waikato.ac.nz/ml/weka/, Accessed on: 15 Aug. 2015.

[54] Measuring vibration. [Online]. Available: http://www.bksv.com/doc/br0094.pdf, Accessed on: 4 Aug. 2016.

[55] M. A. Hall, "Correlation-based feature selection for machine learning," Ph.D. dissertation, Dept. of Comput. Sci., Univ. of Waikato, Hamilton, New Zealand, 1998.

[56] S. Kale, R. Kumar, and S. Vassilvitskii, "Cross-validation and mean-square stability," in *Proc. 25th Int. Conf. Supercomputing*, 31 May-4 Jun. 2011, pp. 487–495.

[57] Lumo back. [Online]. Available: http://www.lumobodytech.com/lumo-back/, Accessed on: 17 Oct. 2017.

[58] Texas instruments simplelink sensortag. [Online]. Available: www.ti.com/sensortag, Accessed on: 17 Oct. 2017.

[59] Fitbit Blaze. [Online]. Available: http://www.electronicproducts.com/Fitbit_Blaze-whatsinside-186.aspx, Accessed on: 30 Nov. 2016.

[60] Fitbit Flex. [Online]. Available: https://www.ifixit.com/Teardown/Fitbit+Flex+Teardown/16050, Accessed on: 30 Nov. 2016.

[61] Cc2650 simplelink mcu. [Online]. Available: http://www.ti.com/lit/ds/symlink/cc2650.pdf, Accessed on: 17 Oct. 2017.

[62] A. Dunkels, B. Gronvall, and T. Voigt, "Contiki-a lightweight and flexible operating system for tiny networked sensors," in *Proc. 29th Annu. IEEE Int. Conf. Local Comput. Netw.*, 2004, pp. 455–462.

[63] F. Büsching, U. Kulau, M. Gietzelt, and L. Wolf, "Comparison and validation of capacitive accelerometers for health care applications," *Comput. Methods Prog. Biomed.*, vol. 106, no. 2, pp. 79–88, 2012.

[64] E. E. Aktakka and K. Najafi, "Three-axis piezoelectric vibration energy harvester," in *Proc. 28th IEEE Int. Conf. Micro Electro Mechanical Syst.*, 2015, pp. 1141–1144.

[65] H. Li, C. Tian, and Z. D. Deng, "Energy harvesting from low frequency applications using piezoelectric materials," *Appl. Physics Rev.*, vol. 1, no. 4, 2014, Art. no. 041301.

Sara Khalifa received the BSc and the MSc degrees in computer science from Zagazig University, Egypt, and the PhD degree in computer science from the University of New South Wales, Sydney, Australia. She is currently a research scientist at Data61|CSIRO, Sydney, Australia. Her current research interests include ubiquitous and pervasive computing, smart wearables, internet of things, energy harvesting, and pattern recognition. She received many awards including the 2017 John Makepeace Bennett award for the Australasian Distinguished Doctoral Dissertation, 2017 NSW iAwards Mobility Innovation of the year, 2017 NSW iAwards Research and Development Project of the year, 2016 Highly Commended Australian NASSCOM Innovation Award, and 2015 CISRA Best Research Paper Award. She is a member of the IEEE.
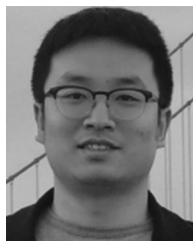
Guohao Lan received the BEng degree in software engineering from the Harbin Institute of Technology, China, and the MS degree in computer science from the Korea Advanced Institute of Science and Technology (KAIST), Korea, in 2012 and 2015. He is currently working toward the PhD degree in the School of Computer Science and Engineering, University of New South Wales (UNSW), Australia. He is also a member of the Networks Research Group, DATA61, CSIRO, Australia. His research interests include wireless networks, mobile and pervasive computing, energy-efficient, and self-powered wearable computing system. He is a student member of the IEEE.

Mahbub Hassan received the MSc degree in computer science from the University of Victoria, Canada, and the PhD degree in computer science from Monash University, Australia. He is a full professor of computer science and engineering, University of New South Wales, Sydney, Australia. He is currently an editor of *IEEE Communications Surveys and Tutorial* and has previously served as guest editor of *IEEE Network* and the *IEEE Communications Magazine*. He was a Distinguished Lecturer of the IEEE (COMSOC) for 2013-2016. His current research interests include pervasive and ubiquitous computing and communication, mobile networking, self-powered wearable computing, and nanoscale wireless networking. More information is available at http://www.cse.unsw.edu.au/~mahbub. He is a senior member of the IEEE.

Aruna Seneviratne received the BEng degree with honors in electrical engineering from Middlesex Polytechnic, and the PhD degree in electrical engineering from the University of Bath, United Kingdom, in 1979 and 1982, respectively. He is currently the Australian Technology Park Laboratory Director and the Leader of Networks Research Group. He holds the Mahanakorn Chair of Telecommunication in the School of Electrical Engineering and Telecommunications, the University of New South Wales. He has more than 15 years of telecommunication and computer systems engineering experience. His research interests include mobile data communication systems, in particular the development of mechanisms for managing the quality of service in wireless Internet environments. Since graduating, he has had rich international experience, having held academic appointments with the University of Bradford, United Kingdom; Curtin University and the Australian Defence Force Academy, University of New South Wales. He is a senior member of the IEEE.

Sajal K. Das received the BS degree from Calcutta University, the MS degree from the Indian Institute of Science, Bangalore and the PhD degree from the University of Central Florida, all in computer science. He is a professor of computer science and Daniel St. Clair Endowed Chair with the Missouri University of Science and Technology, Rolla. His current research interests include wireless sensor networks, smart environments (smart healthcare and smart energy management), cyber-physical systems, mobile and pervasive computing, security and privacy, and social networks. He is a fellow of the IEEE.